OPTICS

Plasmonic linear nanomotor using lateral optical forces

Yoshito Y. Tanaka[1]*, Pablo Albella[2], Mohsen Rahmani[3], Vincenzo Giannini[4], Stefan A. Maier[5,6], Tsutomu Shimura[1]

Optical force is a powerful tool to actuate micromachines. Conventional approaches often require focusing and steering an incident laser beam, resulting in a bottleneck for the integration of the optically actuated machines. Here, we propose a linear nanomotor based on a plasmonic particle that generates, even when illuminated with a plane wave, a lateral optical force due to its directional side scattering. This force direction is determined by the orientation of the nanoparticle rather than a field gradient or propagation direction of the incident light. We demonstrate the arrangements of the particles allow controlling the lateral force distributions with the resolution beyond the diffraction limit, which can produce movements, as designed, of microobjects in which they are embedded without shaping and steering the laser beam. Our nanomotor to engineer the experienced force can open the door to a new class of micro/nanomechanical devices that can be entirely operated by light.

INTRODUCTION

The use of optical force as actuators of micromachines has a huge potential toward the miniaturization and simplification of laboratory-on-a-chip systems (*1*). The optically actuated machines required for such a system including fluid pumps (*2*, *3*), valves (*4*), and mixers (*5*) that are much smaller than those used by other approaches have been individually demonstrated. In particular, conventional approaches using gradient optical force, generated by tightly focusing a laser beam, have enabled various motion actuators (*6*–*9*). However, there are some constraints and limitations: the actuated object's shape and material, the working distances dictated by the geometrical size of the focusing lens, and the spatial resolution of the force distribution due to the light diffraction. Furthermore, they require steering the laser beam for the actuation. These constraints have bottlenecked the integration and implementation of the optically actuated machines.

A simple plane wave also exerts a force on a particle by an exchange of linear and angular momentum during absorbing and scattering processes. While the optical forces decrease with decreasing the particle volume, the forces acting on metal nanoparticles can be remarkably enhanced by localized surface plasmon resonances (*10*–*14*), i.e., collective oscillations of free electrons, enabling the motion control of their host nanoparticles under thermal fluctuations. There have been studies that show the propulsion of the plasmonic particle triggered by a propagating light beam (*15*), evanescent waves (*16*, *17*), and surface plasmon polaritons (*18*) (that is, a linear nanomotor). However, the direction of the propulsion force (radiation pressure) acting on the nanoparticle was restricted to that of the linear momentum flow of the incident waves, i.e., the incident propagation direction, because light scattering by the nanoparticle is isotropic (*19*). Meanwhile, the propulsion force on microparticles can be per-pendicular to the incoming light momentum by controlling the refraction and reflection with their particle shape (*20*, *21*).

Recent theoretical studies (*22*, *23*) have unveiled lateral optical forces acting perpendicular to the incident direction due to asymmetric light scattering of a nanoparticle in consequence of the exchange between spin and orbital angular momenta, but their forces are effective for the particle placed near a surface with the oblique incidence of light. In addition, there has been no experimental demonstration of the lateral forces for nanoparticles, including the plasmonic particles.

Plasmonic nanoparticles can direct the scattered light in a particular direction via engineering of their supported localized plasmon resonances. In particular, multielement nanoparticles with dipolar plasmon resonances at different frequencies allow intense and highly directional scattering (*24*, *25*) even for a normally incident plane wave perpendicular to its propagation direction. Here, we propose a new plasmonic linear nanomotor based on a pair of this detuned dipoles that generates the lateral optical force as the recoil of its unidirectional side scattering. The force direction can be determined by the nanoparticle orientation rather than the incident light direction and the surroundings of the particles. Our experiments demonstrate that the nanomotor allows not only linear but also rotational movement of a micrometer-sized object with different arrangements of the nanoparticles that can control the lateral force distributions with spatial resolution beyond the diffraction limit of light. In principle, we can produce any lateral force distribution just by carefully designing the arrangements and orientations of the nanoparticles.

RESULTS

The underlying principle is as follows: The detuned dipoles oscillate with a phase difference $\Delta\Phi$ due to their different resonance frequencies. When two detuned dipoles are separated by a distance d, the retardation phase kd due to the propagation of their scattered light with wave number k can compensate $\Delta\Phi$ in one direction along the line connecting them and add up in the opposite direction (detailed explanation is provided in section S1). Therefore, careful design of their phase difference $\Delta\Phi$ and separation d enables constructive interference in one direction and destructive interference in the other, i.e., directional side scattering. Figure 1 (A and B) shows a scanning electron microscope image and the extinction spectrum, respectively,

[1]Institute of Industrial Science, University of Tokyo 4-6-1 Komaba, Meguro-ku, Tokyo 153-8505, Japan. [2]Department of Applied Physics, University of Cantabria, Santander, Spain. [3]Advanced Optics and Photonics Laboratory, Department of Engineering, School of Science and Technology, Nottingham Trent University, Nottingham NG11 8NS, UK. [4]Instituto de Estructura de la Materia (IEM), Consejo Superior de Investigaciones Científicas(CSIC), Serrano 121, 28006 Madrid, Spain. [5]Chair in Hybrid Nanosystems, Nanoinstitut München, Fakultät für Physik, Ludwig-Maximilians-Universität München, 80539 München, Germany. [6]Department of Physics, Imperial College London, London SW7 2AZ, UK.
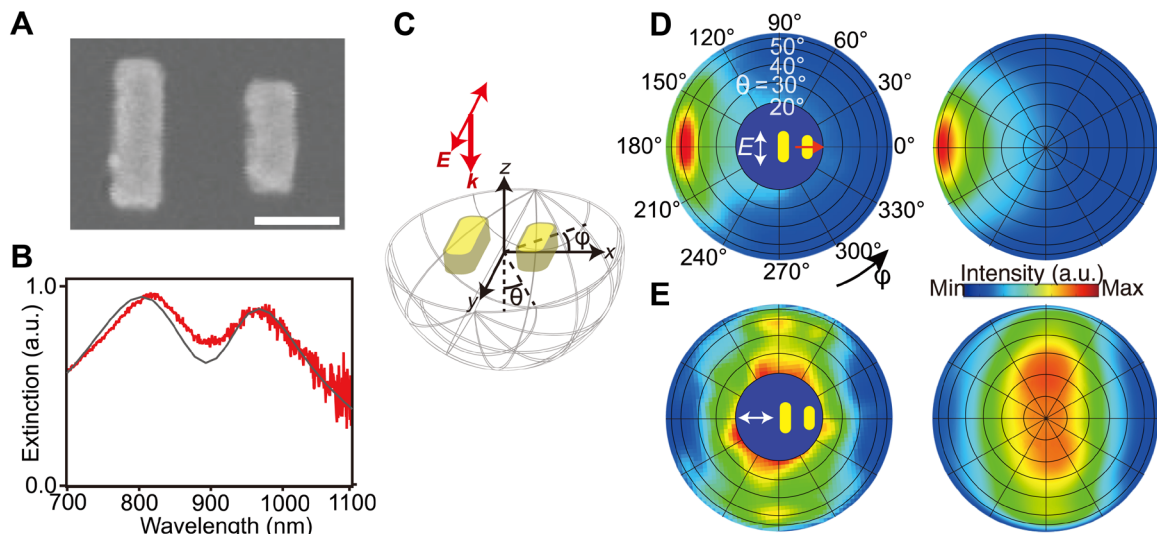*Corresponding author. Email: yoshito@iis.u-tokyo.ac.jp

Fig. 1. A pair of nanoparticles with detuned dipolar resonances to generate lateral optical force. (**A**) Scanning electron microscopy (SEM) image of a pair of gold nanorods with different lengths of 130 and 175 nm. The width and thickness of the nanorods are 60 and 50 nm, respectively. Scale bar, 100 nm. (**B**) Extinction spectra of the pair embedded in silica glass for the experiment (red curve) and calculation (black curve). The different rod lengths separate the resonance peak wavelength. a.u., arbitrary units. (**C**) Illustration of the coordinate system used. (**D** and **E**) Measured (left) and calculated (right) angular distributions of scattered light at the central wavelength between two dipolar resonances for different polarization directions of incident light. In the experiment, the angular distributions with azimuthal angle φ and polar angle θ were obtained using back focal plane imaging (*34*). For incident polarization parallel to the nanorod axis (D), a pair of detuned dipoles exhibits unidirectional side scattering, resulting in a lateral optical force on the nanorod pair (see the inset). When the polarization is rotated by 90° (E), the scattered light pattern changes to almost symmetric, i.e., negligible lateral force. The measured results are in good agreement with numerical calculations.

of a pair of gold nanorods studied in this work. The different nanorod lengths lead to well-separated dipolar plasmon resonances. The scattered light patterns from the asymmetric nanorod pair were measured with the normal incidence of a linearly polarized light beam (Fig. 1C). In the case of the illumination polarization along the nanorod axis, the nanorod pair exhibits strong lateral directionality (Fig. 1D). From the conservation of the light momentum, the nanorod pair would experience a lateral optical force in the opposite direction to its unidirectional side scattering. For the illumination polarization perpendicular to the nanorod axis, the lateral force should be negligible because of the almost symmetric scattering shown in Fig. 1E. Thus, the behavior of the lateral force on the nanorod pair can be controlled by changing the polarization direction of the illumination light.

To demonstrate a plasmonic linear motor based on an asymmetric nanorod pair, a linear array of the pairs in Fig. 2A is embedded in a rectangular silica microblock, as shown in a schematic of Fig. 2B, which reduces its Brownian motion and keeps the configuration of the nanorods in the water environment. In this periodic array, the distance between the pairs along the x axis is determined to enhance the directivity of the scattered light due to the diffraction grating effect (*25*). Figure 2C exhibits consecutive images of the block behavior near the surface of a glass substrate under the normal incidence of a linearly polarized light beam with an intensity of 0.4 mW/μm². The block is confined in the optical focal line generated using a cylindrical lens due to the radiation pressure along the incident light propagation and the optical gradient force perpendicular to the line axis (negligible small along the line). Moreover, the line focus enables the optical alignment of the block along the line axis because of its rectangular geometry. This alignment suppresses the rotational Brownian motion of the block and allows determining the incident polarization direction for the nanorod axis. For the polarization di-

rection along the nanorod axis, the block travels at a velocity of $v_T \sim 6.8$ μm/s along the optical road (see movie S1). When the polarization is rotated by 90°, the linear movement stops quickly (see movie S2). In addition, we confirmed that this linear movement and polarization switching are not observed for the block without the embedded asymmetric nanorod pairs. Note that the illumination light beam carries the linear momentum in its incident direction only, with a zero lateral component in the line axis direction. These show that the linear movement of the block is produced by the lateral force as recoil of the unidirectional side scattering by the asymmetric nanorod pairs, having the light momentum in the line direction.

The block velocity reaches a steady-state velocity in less than 1 ms after changing the illumination polarization, i.e., the lateral force magnitude, as shown in Fig. 2D. In other words, the inertial force is much smaller than the friction forces because of the low Reynolds number in our system. Therefore, the lateral force acting on the microblock, F_{lat}, can be obtained from the equation of motion along the line axis: $f_T v_T = F_{lat}$, where the inertial term is dropped, f_T is the translational friction coefficient, and v_T is the measured velocity of the lateral motion. The friction coefficient f_T can be obtained from the measured mean-squared translational displacement of the Brownian block near the substrate surface (detailed explanation is provided in section S2). In Fig. 2, the nanorod pair array provides a lateral force of $F_{lat} \sim 400$ fN for the polarization direction along the nanorod axis. The numerically calculated lateral optical force exerted on a modeled linear array of asymmetric nanorod pairs is ~900 fN for the same illumination wavelength and intensity as those used in the experiment (calculation method is provided in section S3). Furthermore, as shown in Fig. 2E, the measured velocity v_T, i.e., F_{lat}, increases linearly with the incident light intensity, which is also in good agreement with the behavior of the calculated lateral optical force. Besides, a plasmonic heating effect such as fluid convection
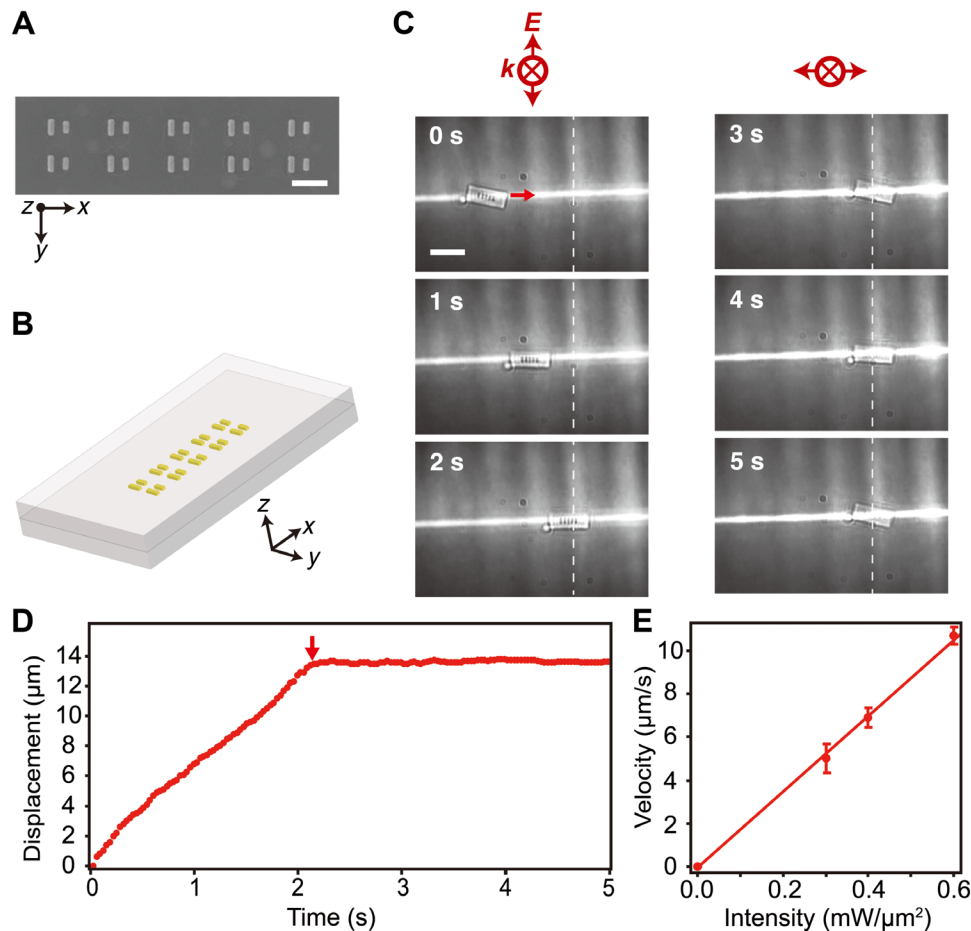
Fig. 2. Direct observation of linear nanomotors. (**A**) SEM image of the nanomotors, a linear array ($\Lambda_x = 660$ nm and $\Lambda_y = 400$ nm) of 10 asymmetric nanorod pairs in Fig. 1A. Scale bar, 400 nm. (**B**) The sample is a 600-nm-thick, 6 μm by 2.5 μm rectangular silica block containing the nanomotors in its center. (**C**) Time sequence of optical microscopy images showing the movement of the sample, provided by the nanomotors, in water under the normal incidence of a linearly polarized light beam (wavelength of 910 nm and intensity of 0.4 mW/μm²). The optical focal line generated using a cylindrical lens aligns the sample along its line axis, enabling control of the incident polarization direction for the nanomotors. Scale bar, 5 μm. (**D**) Translational dynamics of the sample in (C). When the sample arrives at the position, shown by white dashed lines in (C) and a red arrow in (D), the polarization is changed from parallel to perpendicular to the rod axis, while keeping the light intensity constant (see also movie S2). (**E**) Dependence of the measured velocity of the lateral motion on the light intensity. The straight line is linear to fit the data.

should be negligible for the observed lateral motion (detailed explanation is provided in section S4). These support that the lateral optical force acting on the array of nanorod pairs directly causes the linear movement of the block.

The lateral optical force, as well as the directional side scattering, arises from the broken symmetry in the geometry of the nanorod pair so that its force direction is controlled by the pair orientation rather than by the incident direction and polarization of the illuminating light beam. Therefore, the arrangements of the nanorod pairs should allow the lateral force distributions to produce other movements. Figure 3 (A and B) presents circular arrays of the nanorod pairs with different separations, embedded in a square silica microblock as shown in Fig. 3C. In Fig. 3A, the pairs are separated by a distance of ~290 nm smaller than the diffraction limit of roughly $\lambda_{910}/2n_{silica} = 314$ nm, where λ_{910} is the illumination light wavelength of 910 nm and n_{silica} is the refractive index of the silica block. When this pair array is illuminated by a weakly focused linearly polarized laser beam, the block rotates at an angular velocity of $v_R \sim 0.7$ rad/s (Fig. 3, D and F; see also movie S3). The block experiences a torque

of $T = f_R v_R \sim 100$ pN nm, derived from the measured angular velocity v_R and the rotational friction coefficient f_R (detailed explanation is provided in section S2). Since this torque is comparable with the Brownian motion torque $T_B = \sqrt{2\gamma k_B T} \sim 30$ pN nm, where γ is a friction coefficient (26) in water, the fluctuation of the angular velocity still can be seen during the rotation. In the case of the circular array of symmetric nanorod pairs with a resonance at the illumination wavelength, i.e., pairs of tuned dipoles, the block does not rotate in one direction (detailed discussion is provided in section S5). Note that slightly different nanorod lengths produce the obvious difference of the rotational behavior. Thus, the unidirectional rotation is a result of the torque generated by detuned dipoles, and it does not arise from the surface roughness of the microblock or a plasmonic heating effect such as fluid convection.

Conventional plasmonic rotary motors (26–29) consist of a single nanoparticle that directly experiences an optical torque due to the transfer of angular momentum carried by the incident light or the scattered light. On the other hand, the rotation produced by our nanomotor is based on the torque due to the circular distribution of
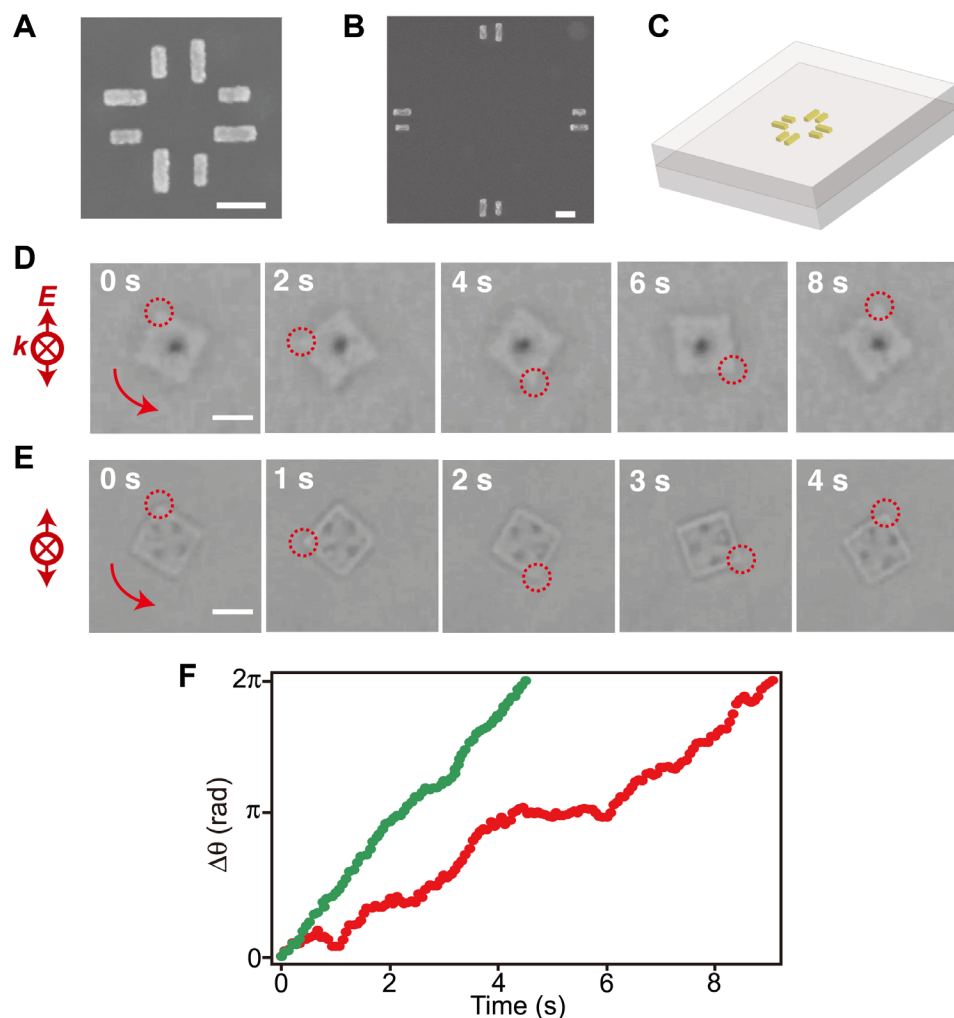
Fig. 3. Rotation produced by the nanomotors. (**A** and **B**) SEM images of circular arrays of the nanomotors with different separations of 290 nm (A) and 1340 nm (B). Scale bars, 200 nm, respectively. (**C**) The sample is a 600-nm-thick, 2.5-μm by 2.5-μm square block containing the nanomotors. (**D** and **E**) Nanomotors of (A) and (B), respectively, rotate the microblock under the normal incidence of a linearly polarized light beam at a wavelength of 910 nm (see movies S3 and S4). The dashed red circles in the two series indicate the same corner of the block. Although a single dark spot in the sample of (D) shows the nanomotors, the individual ones cannot be resolved because of the diffraction limit. The light intensities for (D) and (E) are 4.5 and 2 mW/μm², respectively. Scale bars, 2 μm. (**F**) Rotational dynamics of the samples in (D) (red dots) and (E) (green dots). For the larger separation between the nanomotors, the sample rotates at almost double angular velocity even with less than half the light intensity, which shows the enhancement of the torque by increasing the distance between the array center and the individual nanomotors.

the lateral optical force on the nanorod pair. Therefore, the magnitude of the torque can be enhanced simply by increasing the distance between the center of the circular array and the individual pairs. A microblock with just an increased pair separation of Fig. 3B rotates at double speed with less than half of the light intensity while keeping the whole volume of the nanoparticles (Fig. 3, E and F; see also movie S4).

To gain further insight into the observed rotation, we show the dependence of the angular velocity of the rotated block on the illumination wavelength in the relation with the measured extinction spectrum of the nanorod pairs (Fig. 4). The angular velocity has a single peak at the wavelength between two plasmon resonances, which is different from the conventional plasmonic motors whose torques have a positive correlation with their resonances. It should be noted that its spectral behavior also does not correspond to wavelength dependences of any conventional optical forces on

nanoparticles: gradient forces and scattering forces including the conventional lateral forces that are directly proportional to real and imaginary parts of the nanoparticle polarizability, respectively. On the other hand, there is good agreement of the spectral behavior between the angular velocity and the lateral force on a single asymmetric nanorod pair in the inset of Fig. 4 that is determined by the lateral directionality of the scattered light rather than the particle polarizabitliy (see wavelength dependence of directivity of the scattered light in section S6). Thus, this result strongly supports that the lateral force distribution controlled by the arrangement of the pairs produces the rotational movements.

DISCUSSION
We have revealed that lateral optical forces on asymmetric nanorod pairs due to directional side scattering can produce controlled
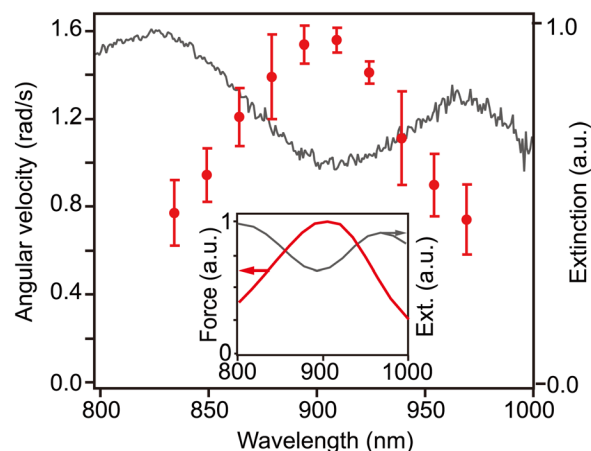
Fig. 4. Wavelength dependence of angular velocity of the rotating sample. The sample is the same as in Fig. 3E. The angular velocity has a spectral peak at a wavelength between two plasmon resonances in the measured extinction spectrum (gray curve) of the nanomotors, which corresponds to a peak wavelength of calculated lateral force on a single asymmetric nanorod pair in the inset. The lateral force has a positive correlation with the directivity of the scattered light (see fig. S7).

movements of a micrometer-sized silica block in which they are embedded by overcoming the Brownian forces. The arrangements and orientations of the pairs allow controlling the lateral force distributions with spatial resolution beyond the diffraction limit of light, resulting in not only linear but also rotational movements of the microblocks under the normal incidence of a linearly polarized light beam. In other words, instead of tailoring the incident light beam, we use the embedded pairs to engineer the optical force experienced by the block. This plasmonic nanomotor can be driven even by an incident plane wave with zero linear and angular momentum. It would provide a paradigm shift in optical manipulation as it removes the limitation of light diffraction and the need for oblique incidence, shaping, and steering of the light beam. Moreover, our method relaxes constraints of the manipulated object such as the shape and permittivity (refractive index) because the optical force is induced by the interaction between light and the nanoparticles attached to the object.

The recent invention of plasmonic nanoantennas has led to designs that not only direct scattered light but also directionally steer it according to the parameters of the incident light, e.g., frequency (30–33) and polarization (34). Therefore, these nanoantennas would allow us to navigate the motor by controlling the direction and magnitude of the lateral optical forces with the frequency, polarization, and intensity of the incident light. Furthermore, when we design multiple motors that work at different resonance frequencies and produce different movements, e.g., linear and rotational movements, their movements can be switched by changing the incident light frequencies from the one resonance to the other. For efficiently driving the motors in this study, we used the shaped light beams to restrict the degrees of freedom of the motion. When the motors are situated into microchannels, a simple plane wave would be sufficient to efficiently drive them because we can control the degrees of freedom of the motion via the shape and size of the microchannels. Thus, our unique approach can provide a powerful tool for creating complex, highly integrated, microscale total analysis systems. We also envision novel optomechanical nanodevices with dynamic control of nanoscale

stress distributions, including tunable metamaterials (35) and graphene devices (36).

MATERIALS AND METHODS

Fabrication of nanomotors embedded in microblocks

The samples were fabricated by electron beam lithography (EBL) and dry etching techniques (26). The whole fabrication process can be described as follows: A 200-nm-thick silicon layer (a sacrificial layer) was deposited on a coverslip substrate by sputtering, followed by a 300-nm SiO_2 layer (fig. S1A). A positive resist film for EBL was formed by spin coating with a thickness of 200 nm on the substrate. The film was exposed to a given pattern of nanostructures using an EBL system with a high accelerating voltage (125 kV) and then developed. A 50-nm gold layer was deposited by electron-beam evaporation. The resist pattern was subsequently removed from the substrate, resulting in the formation of the gold nanostructures on the SiO_2 layer (fig. S1B). Additional 300-nm SiO_2 layer was deposited to sandwich the nanostructures between two SiO_2 layers (fig. S1C). The sample was then coated with the resist to define the microblock by a second EBL process. A 50-nm aluminum layer was used as a mask of the microblock for the etching of SiO_2 with CHF_3, and it was removed by aluminum etchant (fig. S1, D to F). At the last step, the sacrificial silicon layer was removed by dry etching with XeF_2 to release the sample from the substrate to water (fig. S1G).

Experimental procedures

The sample on a coverslip surface was released into water between two coverslips, and it moved from the top coverslip to the bottom due to the gravitational force. The Brownian motion of the sample can be seen near the surface of the bottom coverslip. The sample concentration is at most 30 samples/μl, and the samples are always isolated in the cell. A continuous-wave Ti-Sapphire laser beam was used for driving the nanomotors. The sample was illuminated by the linearly polarized beam at the normal incidence from the top, as shown in fig. S2. The illumination of the laser beam and the observation of the sample were performed using different lenses to increase their flexibility. For the experiment of the linear movement of the sample, the optical focal line to confine and align the sample was generated by a cylindrical lens (fig. S2A). The polarization of the laser beam was rotated using a half-wave plate. For the experiment of the sample rotation, the laser beam was weakly focused with a spot size of ~10 μm to obtain uniform illumination (fig. S2B). The sample motion was observed by an inverted microscope equipped with a high numerical aperture (NA) water immersion objective (60×, NA = 1.2), enabling the analysis of the microblock behavior with the high spatial resolution.

SUPPLEMENTARY MATERIALS

Supplementary material for this article is available at http://advances.sciencemag.org/cgi/content/full/6/45/eabc3726/DC1

REFERENCES AND NOTES

1. J. Glückstad, Microfluidics: Sorting particles with light. *Nature Mater.* **3**, 9–10 (2004).
2. S. Maruo, H. Inoue, Optically driven micropump produced by three-dimensional two-photon microfabrication. *Appl. Phys. Lett.* **89**, 144101 (2006).
3. S. Maruo, H. Inoue, Optically driven viscous micropump using a rotating microdisk. *Appl. Phys. Lett.* **91**, 084101 (2007).
4. A. Terray, J. Oakey, D. W. M. Marr, Microfluidic control using colloidal devices. *Science* **296**, 1841–1844 (2002).

5. S. L. Neale, M. P. Macdonald, K. Dholakia, T. F. Krauss, All-optical control of microfluidic components using form birefringence. *Nat. Mater.* **4**, 530–533 (2005).

6. S. Kawata, H.-B. Sun, T. Tanaka, K. Takada, Finer features for functional microdevicecs. *Nature* **412**, 697–698 (2001).

7. D. G. Grier, A revolution in optical manipulation. *Nature* **424**, 810–816 (2003).

8. D. Palima, J. Glückstad, Gearing up for optical microrobotics: Micromanipulation and actuation of synthetic microstructures by optical forces. *Laser Photon. Rev.* **7**, 478–494 (2013).

9. U. G. Būtaitė, G. M. Gibson, Y.-L. D. Ho, M. Taverne, J. M. Taylor, D. B. Phillips, Indirect optical trapping using light driven micro-rotors for reconfigurable hydrodynamic manipulation. *Nat. Commun.* **10**, 1215 (2019).

10. H. Xu, M. Käll, Surface-plasmon-enhanced optical forces in silver nanoaggregates. *Phys. Rev. Lett.* **89**, 246802 (2002).

11. P. M. Hansen, V. K. Bhatia, N. Harrit, L. Oddershede, Expanding the optical trapping range of gold nanoparticles. *Nano Lett.* **5**, 1937–1942 (2005).

12. Y. Tanaka, H. Yoshikawa, T. Itoh, M. Ishikawa, Laser-induced self-assembly of silver nanoparticles via plasmonic interactions. *Opt. Express* **17**, 18760–18767 (2009).

13. M. J. Guffey, R. L. Miller, S. K. Gray, N. F. Scherer, Plasmon-driven selective deposition of Au bipyramidal nanoparticles. *Nano Lett.* **11**, 4058–4066 (2011).

14. A. Lehmuskero, P. Johansson, H. Rubinsztein-Dunlop, L. Tong, M. Käll, Laser trapping of colloidal metal nanoparticles. *ACS Nano* **9**, 3453–3469 (2015).

15. A. H. J. Yang, T. Lerdsuchatawanich, D. Erickson, Forces and transport velocities for a particle in a slot waveguide. *Nano Lett.* **9**, 1182–1188 (2009).

16. S. Kawata, T. Tani, Optically driven Mie particles in an evanescent field along a channeled waveguide. *Opt. Lett.* **21**, 1768–1770 (1996).

17. M. Ploschner, T. Čižmár, M. Mazilu, A. Di Falco, K. Dholakia, Bidirectional optical sorting of gold nanoparticles. *Nano Lett.* **12**, 1923–1927 (2012).

18. K. Wang, E. Schonbrun, K. B. Crozier, Propulsion of gold nanoparticles with surface plasmon polaritons: Evidence of enhanced optical force from near-field coupling between gold particle and gold film. *Nano Lett.* **9**, 2623–2629 (2009).

19. J. J. Sáenz, Optical forces: Laser tractor beams. *Nat. Photon.* **5**, 514–515 (2011).

20. G. A. Swartzlander Jr., T. J. Peterson, A. B. Artusio-Glimpse, A. D. Raisanen, Stable optical lift. *Nat. Photon.* **5**, 48–51 (2011).

21. A. Búzás, L. Kelemen, A. Mathesz, L. Oroszi, G. Vizsnyiczai, T. Vicsek, P. Ormos, Light sailboats: Laser driven autonomous microrobots. *Appl. Phys. Lett.* **101**, 041111 (2012).

22. S. B. Wang, C. T. Chan, Lateral optical force on chiral particles near a surface. *Nat. Commun.* **5**, 3307 (2014).

23. F. J. Rodríguez-Fortuño, N. Engheta, A. Martínez, A. V. Zayats, Lateral forces on circularly polarizable particles near a surface. *Nat. Commun.* **6**, 8799 (2015).

24. T. Kosako, Y. Kadoya, H. F. Hofmann, Directional control of light by a nano-optical Yagi–Uda antenna. *Nat. Photon.* **4**, 312–315 (2010).

25. A. B. Evlyukhin, S. I. Bozhevolnyi, A. Pors, M. G. Nielsen, I. P. Radko, M. Willatzen, O. Albrektsen, Detuned electrical dipoles for plasmonic sensing. *Nano Lett.* **10**, 4571–4577 (2010).

26. M. Liu, T. Zentgraf, Y. Liu, G. Bartal, X. Zhang, Light-driven nanoscale plasmonic motors. *Nat. Nanotechnol.* **5**, 570–573 (2010).

27. L. Shao, Z.-J. Yang, D. Andrén, P. Johansson, M. Käll, Gold nanorod rotary motors driven by resonant light scattering. *ACS Nano* **9**, 12542–12551 (2015).

28. A. Lehmuskero, R. Ogier, T. Gschneidtner, P. Johansson, M. Käll, Ultrafast spinning of gold nanoparticles in water using circularly polarized light. *Nano Lett.* **13**, 3129–3134 (2013).

29. L. Shao, M. Käll, Light-driven rotation of plasmonic nanomotors. *Adv. Funct. Mater.* **28**, 1706272 (2018).

30. T. Shegai, S. Chen, V. D. Miljković, G. Zengin, P. Johansson, M. Käll, A bimetallic nanoantenna for directional colour routing. *Nat. Commun.* **2**, 481 (2011).

31. P. Albella, T. Shibanuma, S. A. Maier, Switchable directional scattering of electromagnetic radiation with subwavelength asymmetric silicon dimers. *Sci. Rep.* **5**, 18322 (2015).

32. J. Li, N. Verellen, D. Vercruysse, T. Bearda, L. Lagae, P. V. Dorpe, All-dielectric antenna wavelength router with bidirectional scattering of visible light. *Nano Lett.* **16**, 4396–4403 (2016).

33. R. Guo, M. Decker, F. Setzpfandt, I. Staude, D. N. Neshev, Y. S. Kivshar, Plasmonic Fano Nanoantennas for on-chip separation of wavelength-encoded optical signals. *Nano Lett.* **15**, 3324–3328 (2015).

34. Y. Y. Tanaka, T. Shimura, Tridirectional polarization routing of light by a single triangular plasmonic nanoparticle. *Nano Lett.* **17**, 3165–3170 (2017).

35. N. I. Zheludev, Y. S. Kivshar, From metamaterials to metadevices. *Nat. Mater.* **11**, 917–924 (2012).

36. C. Si, Z. Sun, F. Liu, Strain engineering of graphene: A review. *Nanoscale* **8**, 3207–3217 (2016).

37. A. P. Philipse, *Brownian Motion: Elements of Colloid Dynamics* (Springer, 2018).

38. J. S. Donner, G. Baffou, D. McCloskey, R. Quidant, Plasmon-assisted optofluidics. *ACS Nano* **5**, 5457–5462 (2011).

39. G. Baffou, R. Quidant, C. Girard, Thermoplasmonics modeling: A Green's function approach. *Phys. Rev. B* **82**, 165424 (2010).